Mechanistic insights into zearalenone-accelerated colorectal cancer in mice using integrative multi-omics approaches

Emily Kwun Kwan Lo[1†], Xiuwan Wang[2†], Pui-Kei Lee[3], Ho-Ching Wong[3], Jetty Chung-Yung Lee[1], Carlos Gómez-Gallego[4], Danyue Zhao[3,5*], Hani El-Nezami[1,4] and Jun Li[2,6*]

[1]School of Biological Sciences, University of Hong Kong, Pokfulam 999077, Hong Kong, China
[2]Department of Infectious Diseases and Public Health, Jockey Club College of Veterinary Medicine and Life Sciences, City University of Hong Kong, Kowloon Tong, Hong Kong 999077, China
[3]Department of Applied Biology and Chemical Technology, The Hong Kong Polytechnic University, Hong Kong
[4]Institute of Public Health and Clinical Nutrition, School of Medicine, University of Eastern Finland, FI-70211 Kuopio, Finland
[5]Research Institute for Future Food, The Hong Kong Polytechnic University, Hong Kong
[6]School of Data Science, City University of Hong Kong, Hong Kong, China

† These authors have contributed equally to this work and share first authorship
*Correspondence: jun.li@cityu.edu.hk (J.L.), daisydy.zhao@polyu.edu.hk (D.Z.)

Summary

Zearalenone (ZEA), a secondary metabolite from *Fusarium* fungi found in cereal-based foods, promotes the growth of colon, breast, and prostate cancers *in vitro*. However, the lack of animal studies hinders a deeper mechanistic understanding of the cancer promotive effect of ZEA. The aim of this study was to unveil the effect of ZEA on colon cancer progression and its underlying mechanism. Through integrative analyses of transcriptomics, metabolomics, metagenomics, and host phenotypes, we investigated the impact of a 4-week ZEA intervention on colorectal cancer in xenograft mice. Our results showed that a 4-week ZEA intervention increased the tumor weight twofold. ZEA exposure significantly increased the mRNA and protein levels of BEST4, DGKB and KI67, and the phosphorylation levels of ERK1/2 and AKT. Metabolomics analysis of the serum revealed the levels of amino acids, including histidine, arginine, citrulline and glycine decreased significantly in the ZEA group. Furthermore, ZEA lowered the alpha diversity of the gut microbiota and reduced the abundance of 9 genera, such as *Tuzzerella* and *Rikenella*, etc. Further association analysis indicated that *Tuzzerella* was negatively associated with the expression of BEST4 and DGKB genes, serum uric acid level and tumor weight. In addition, circulatory hippuric acid level was positively correlated with the tumor weight and the expression of oncogenic genes, including ROBO3, JAK3 and BEST4. Altogether, our results indicated that ZEA promoted colon cancer tumor progression through enhancing the BEST4/AKT/ERK1/2 pathway, lowering the circulatory amino acid concentration, alternating the gut microbiota composition, and suppressing the SCFA production.

Keywords

Zearalenone, colon cancer, RNA-Seq, gut microbiota, metabolomics, multi-omics

Introduction

Colorectal cancer (CRC) is one of the most common cancers and the third leading cause of cancer death [1], while the pathogenesis of CRC is still undergoing active exploration. Exogenous estrogen exposure has been classified as an environmental hazard, contributing to CRC progression through binding to estrogen receptors [2]. Zearalenone (ZEA) is a mycotoxin commonly found in our diet, mainly in cereals and grains. ZEA is a secondary metabolite produced by *Fusarium* species. Due to its structural similarity to estrogen, studies on ZEA carcinogenicity have therefore focused on hormone-dependent cancers. A recent epidemiological study discovered a link between increased urinary ZEA metabolites and the development of breast cancer [3]. Furthermore, ZEA has been implicated in promoting cancer cell growth and progression in breast [4], prostate [5] and colon cancer cells [6, 7] *in vitro*. These investigations, however, disregarded the three-dimensional growth, microenvironment of tumors, and immunoregulatory role of the gut microbiota in living animals [8]. To the best of our knowledge, there is no *in vivo* study evaluating the impact of ZEA on CRC.

In recent years, increasing evidence suggests that dysbiosis in the gut microbiome may contribute to CRC development [9-11]. The microenvironment of CRC is a complex community composed of cancer cells and microorganisms [12]. Previous studies have shown that the gut microbiota shapes immune responses and promotes tumor growth [13]. Since ZEA is mainly digested and absorbed through the gastrointestinal tract, the gut microbiota is directly exposed to ZEA and potentially regulates the metabolism and carcinogenesis of ZEA [14]. Indeed, studies have indicated that ZEA disrupts the composition and function of the gut microbiota in healthy animals [15-17].

61 In this study, using combined analyses of the tumor transcriptome, targeted and untargeted
62 metabolomics and 16S rDNA sequencing, we comprehensively evaluated the impact of ZEA
63 exposure on the development and progression of CRC in a colon cancer xenograft mouse model.
64 We aimed to investigate the underlying mechanisms related to accelerated tumor growth and
65 identify the key transcriptional signature, gut microbes, and metabolites that potentially contribute
66 to ZEA-induced colon cancer development.

67

68 **Materials and Methods**

69 *Animal study*

70 Nude BALB/cAnN mice were purchased from the Laboratory Animal Unit of the University
71 of Hong Kong. Five-week-old male mice were housed in individual ventilated cages in a sterile
72 environment with regulated temperature (23-24ºC) and relative humidity (60-70%) on a 12-hour
73 light cycle. The mice were fed a phytoestrogen-free diet (Open Standard diet, D11112201,
74 Research Diets Inc., New Brunswick, NJ) and water provided *ad libitum*. After one week of
75 acclimatization, the mice were injected in the right flank with $1x10^6$ SW480 human colon cancer
76 cells mixed with PBS/Matrigel (1:1). When the tumor size reached 70-100 mm^3, the mice were
77 randomly divided into two treatment groups (n=9 per group): control [oral gavage vehicle (olive
78 oil) thrice weekly] or ZEA (0.5 mg/kg body weight (BW) in olive oil thrice weekly) (Figure 1A).
79 The dosage in this study was chosen based on an animal study in which 1 mg/kg BW ZEA
80 promoted DNA adduct formation in healthy mice, and the reported levels of ZEA in grain-based
81 food in humans (3.0-33.0 μg/kg bw/day) [14, 18], in which 33.0 μg/kg bw/day was converted
82 through body surface area conversion from humans to mice [19]. The measurement of tumor size
83 was made as previously described with modification [20]. The sizes of tumors were measured by

84 an electric caliper thrice weekly. Tumor volumes were calculated based on the formula: volume
85 (mm^3) = (π x length (mm) × width $(mm)^2$)/6. The length represents the longest tumor diameter,
86 and the width represents the perpendicular tumor diameter. BW and food consumption were
87 recorded thrice weekly throughout the study. After 28 days, the mice were sacrificed with
88 pentobarbital (250 mg/kg, intraperitoneal injection), and the tumors and caecal contents were
89 removed, weighed and snap frozen in liquid nitrogen. Animal handling for the experimentation
90 was approved by the Committee on the Use of Live Animals in Teaching and Research (CULATR
91 No. 4785-18), the University of Hong Kong.

92

93 *RNA extraction and RNA-seq*

94 Total RNA was isolated from the tumor tissue using an RNAspin Mini kit (GE Healthcare,
95 UK) according to the manufacturer's instructions. After passing the quality check, the samples
96 were fragmented and reversely transcribed to cDNA. The final cDNA library was then built by
97 Novogene (Novogene, China) through the following procedure: purification, terminal repair, A-
98 tailing, ligation of sequencing adapters, size selection and PCR enrichment. Finally, reads were
99 generated using Illumina HiSeq 2500.

100

101 *Quality control of RNA-Seq reads and quantification of gene expression*

102 We mapped all raw reads to the GRCm38 (Genome Reference Consortium Mouse Build 38,
103 NCBI BioProject Accession: PRJNA20689) genome using BWA v0.7.17 and removed those with
104 more than 95% mapping coverage. The ribosomal RNA (rRNA) reads were filtered with
105 SortMeRNA [21]. Raw reads were further processed for quality control using the following

106 procedures [22] (available at
107 https://github.com/TingtZHENG/metagenomics/blob/master/scripts/fqc.pl): (i) Illumina
108 primers/adaptors/linker sequences were removed; (ii) paired-end reads with 25 bp consecutively
109 exact matches from both ends were removed to avoid PCR duplicates; and (iii) terminal regions
110 with continuous Phred-based quality less than 20 were removed. High-quality remaining reads
111 were aligned using TopHat2 v2.1.1 employing the GRCh38 (Genome Reference Consortium
112 Human Build 38, NCBI BioProject Accession: PRJNA31257) assembly as the human reference
113 genome. Thereafter, alignment outputs from TopHat2 were formatted and sorted with SAMtools
114 v1.9. SAMtools outputs were used to perform gene counts using the htseq-count function from
115 HTseq framework v0.11.2. In addition, RSEM v1.3.1 was executed to estimate fragments per
116 kilobase of transcript per million mapped reads (FPKM) based on the alignment results. Based on
117 the read count of genes for each sample, we first applied centered log-ratio (clr) transformation.

118

119 *Analysis of differentially expressed genes and enriched pathways*

120 Subsequently, differentially expressed genes were identified by DESeq2 v1.34.0, which
121 calculated the significance of gene expression profile alternations in comparison groups. The
122 adjusted p-value < 0.1 were used as the cutoff values for significantly differentially expressed
123 genes. Next, differentially expressed pathways were identified by Generally Applicable Gene-set
124 Enrichment (GAGE, v2.44.0) analysis using gene sets derived from KEGG pathways. An adjusted
125 p-value < 0.1 was used to define significantly differentially expressed pathways in the comparison
126 groups. In addition, Gene set enrichment analysis (GSEA, v4.0.3) was performed on gene
127 expression profiles using gene sets from the Molecular Signatures Database (MSigDB, v7.1): (1)

128 Cancer Hallmarks, (2) Oncogenic Signatures and (3) Chemical and Genetic Perturbations. |NES
129 score| > 1 and FDR < 0.25 were used as the cutoff values for significantly enriched gene sets.

130

131 *Hematoxylin-eosin (H&E) staining, immunohistochemistry (IHC) and TUNEL assay*

132 A part of the tumor tissue was washed, fixed immediately with formalin and embedded in
133 paraffin for sectioning into 5 mm slices. The sections were then deparaffinized and used to conduct
134 H&E staining, IHC, or TUNEL fluorescent staining. H&E staining was performed using H&E kit
135 from Baso (Zhuhai, China) according to the manufacturer's recommendations. The TUNEL assay
136 was performed using In Situ Cell Death Detection Kit (Roche Diagnostics) according to the
137 manufacturer's instructions with modification [23]. In brief, the slides were incubated in 0.1 M
138 citrate buffer in a 70°C water bath for 30 minutes and then blocked with CAS block (Thermo
139 Fisher, USA). The slides were washed and then incubated with TUNEL reaction mixture for 60
140 min at 37°C. For IHC, the sections were rehydrated in graded alcohols and distilled water. It was
141 then boiled in Tris-EDTA followed by quenching endogenous peroxidase activities using 3%
142 H2O2. The sections were immersed in CAS-Bloc Histochemical Reagent (Thermo Fisher, USA)
143 and incubated with primary antibodies against pERK1/2, pAKT, Ki67, BEST4, (1:100, Abcam)
144 and DGKB (Invitrogen, USA) at 4°C overnight. It was then washed thoroughly and incubated with
145 anti-mouse or anti-rabbit HRP-conjugated secondary antibody (Bio-Rad) or anti-goat HRP-
146 conjugated secondary antibody (Bio-Rad). Positive signals were visualized using 3,3'-
147 diaminobenzidine (Abcam, USA). The nuclei were counterstained with hematoxylin. Expression
148 in IHC images was quantified by NIH ImageJ v1.50 software as described in [24].

149

150 *Non-targeted metabolomics analysis*

151 One hundred microliters of serum sample were added to 1 mL ice-cold 100% methanol, spiked
152 with 4-chloro-phenylalanine as the internal standard at a final concentration of 100 ng/mL. The
153 mixture was vortexed for 30 s and kept at -20°C for 20 min. The cold mixture was then centrifuged
154 at 17,000 x g at 4°C for 15 min. The supernatant was collected and dried under a gentle flow of
155 nitrogen. The dried samples were reconstituted with 100 μL 60% methanol and sonicated for 1
156 min before centrifugation at 17,000 x g for 10 min. The supernatant collected was subjected to
157 LC–MS/MS analysis using Agilent 6540 UHPLC-QTOF-MS/MS (Agilent Technologies, Santa
158 Clara, CA, USA) with a Waters ACQUITY HSS T3 column, 2.1 mm × 100 mm, 1.7 μm (Milford,
159 MA). The column temperature was set at 40°C and the injection volumes for positive mode and
160 negative mode were set at 10 μL and 15 μL, respectively. The mobile phases consisted of water
161 with 0.1% formic acid (A) and acetonitrile with 0.1% formic acid (B) at a flow rate of 0.3 mL/min.
162 The gradient (B%) started with 1% from 0 to 1 min and increased to 99% from 1 min to 10 min,
163 holding at 99% until 13 min and then returned to 1% at 13.5 min and maintained until 16 min. The
164 MS parameters were as follows: capillary voltage 4000 V, nozzle voltage 1500 V, skimmer voltage
165 65 V, drying gas temperature 300°C, sheath gas temperature 320°C, fragmentor voltage 140 V,
166 drying gas flow rate 8 L/min, sheath gas flow rate 11 L/min, and nebulizer pressure 40 psi. The
167 metabolites were identified by comparing the data to the HMDB and METLIN databases using
168 Progenesis QI software version 3.0 (Nonlinear Dynamics, Newcastle, UK).

169

170 *Targeted metabolomics for amino acid profiling*

171 Serum samples (50 μL) were mixed with 50 μL internal standard (Kairos Amino Acid Internal
172 Standard Set, Waters USA) and water according to the manufacturer's instructions. The mixture

173 was then centrifuged at 9000 x g for 15 min. The mixture (10 μL) was then mixed with 70 μL of
174 borate buffer and 10 μL of AccQ•Tag reagent. After vortexing for 5 s, the mixture was allowed to
175 stand at room temperature for 1 min and heat for 10 min at 55°C. The mixture was then analyzed
176 using Agilent 6460 UHPLC-QqQ-MS/MS (Agilent Technologies, Santa Clara, CA, USA) with a
177 Waters Cortecs C18 column, 2.1 mm × 150 mm, 1.6 μm (Milford, MA). For chromatographic
178 separation, a binary mobile phase system was used including 0.1% formic acid in water (A) and
179 0.1% formic acid in acetonitrile (B) with a flow rate of 0.5 mL/min. The gradient elution program
180 (B%) for each run started at 1%, lasted for 1 min, and then increased to 13% at 2 min, 13% to 15%
181 from 2 to 5.5 min, 15% to 95% from 5.5 to 6.5 min, kept at 95% until 7.5 min, then decreased to
182 1% from 7.5 min to 7.6 min and maintained at 1% until 9 min. The column temperature was 55°C,
183 and the injection volume was 2 μL. Data processing was achieved using Agilent MassHunter
184 Workstation software (version B.06.00).

185

186 *Metabolomics data analysis*

187 Pathway analysis was performed to integrate the targeted amino acid results using the
188 Ingenuity Pathway Analysis Software (IPA) version 70750971 (QIAGEN, Redwood City, USA).
189 Metabolites strongly correlated with tumor weight were identified by Spearman's rank correlation
190 analysis. The |correlation| > 0.6 and *p-value* < 0.05 were used as the cutoff values of statistical
191 significance.

192

193 *Total microbial DNA extraction and 16S rDNA gene quantitative analysis*

194 The DNA content of the caecal samples was extracted using a DNeasy Powersoil Kit (Qiagen,
195 Germany) according to the manufacturer's instructions. The quality of extracted DNA samples
196 was examined through 1% agarose gel electrophoresis. The DNA samples were then sent to
197 Novogene Co. Ltd (Beijing, China) for sequencing. After quality check, the hypervariable region
198 V3-V4 (341F&534R) of the 16S rDNA was amplified. PCR was then performed by Phusion High-
199 Fidelity PCR master mix (New English Biolabs, England). The PCR product was quantified with
200 2% agarose electrophoresis gel. The products between 400 and 450 bp were extracted by Qiagen
201 Gel Extraction Kit (Qiagen, Germany). Samples were quantified through Qubit and prepared for
202 sequence library generation by the NEBNext Ultra DNA library prep kit. The resulting library was
203 then sequenced on the Illumina HiSeq 2500 platform. The R package dada2 v1.22.0 was used to
204 perform read quality control and resolve amplicon sequence variants (ASVs). Thirty low-quality
205 3' bases of the forward and reverse reads were removed following inspection of QC plots. Reads
206 with any Ns or a maximum expected error of > 2 following truncation and mapping to phiX were
207 also removed. Error estimation was calculated on all samples (pooled) following dereplication.
208 After that, dada2 merged overlapping forward and reverse reads, and then removed chimeric
209 sequences. Following chimera removal, taxonomy was assigned independently to the SILVA
210 v138.1 reference database. Next, Shannon diversity at the genus level was calculated with the R
211 package vegan v2.6.2. Furthermore, the alpha diversity indexes were compared between the
212 experimental and control groups using independent-sample t-test. The R package vegan and
213 compositions v2.0.4 [25] were used to calculate beta diversity based on robust Aitchison distance.
214 The Wilcoxon rank sum test was used to evaluate whether there was significant difference for pair-
215 wise distance within groups between comparison groups. We then evaluated beta diversity in

216 multiple dimension scale (MDS) ordinations with vegan. Moreover, permutational multivariate
217 analysis of variances (PERMANOVA) of the distance matrices between groups was performed to
218 calculate R values (0 = no difference; 1 =maximum dissimilarity) to determine dissimilarities
219 among groups. Differential abundance of taxa at the genus level between comparison groups was
220 completed using Analysis of Compositions of Microbiomes with Bias Correction (ANCOM-BC)
221 implemented in R package ANCOMBC v1.4.0 [26]. An adjusted *p value* < 0.05 was used as the
222 cutoff to define significantly differentially abundant genera between groups.

223

224 *Gene expression, microbiota, and metabolome integrative analysis*

225 We performed an integrative analysis to reveal the associations among multi-omics and
226 phenotypic data. First, Spearman's correlation coefficients between the differentially expressed
227 genes, differentially abundant microbial taxa and differentially abundant metabolites between the
228 experimental and control groups were calculated. Statistical significance was set as FDR < 0.05
229 after Bonferroni correction, and a strong correlation was defined as |correlation|>0.8. Furthermore,
230 we built the significant strong correlations into a visualization network using Cytoscape software
231 v3.9.1.

232

233 *Short chain fatty acids (SCFAs) analysis of caecal contents*

234 The concentration of SCFAs in the caecum was measured by gas chromatography–mass
235 spectrometry (GC–MS) as previously described with modification [27, 28]. In brief, the caecal
236 content samples were homogenized using a blade homogenizer (T25, ULTRA-TUREAX, IKA) in
237 an extraction buffer containing 0.005 M sodium hydroxide with internal standard (10 μg/ml

238 deuterated acetic acid, acetic acid-d4). The homogenates were centrifuged at 13,200 x g for 20 min
239 at 4°C. The supernatant was mixed with 0.5 ml of 1-propanol/pyridine (3:2, v:v) and 0.1 ml of
240 propyl chloroformate. The mix was vortexed for 1 min and incubated at 60°C to derivatize the
241 SCFAs. The derivatized samples were then mixed with 0.5 ml hexane and centrifuged at 2000 x g
242 for 4 min. Thereafter, 400 µl of the upper layer was transferred to a glass vial for GC–MS analysis
243 (Agilent 6890N-5973 GC–MS, USA) set according to Zheng et al [27] report. The concentration
244 of SCFAs was quantified using the calibration curves constructed using acetic acid, propionic acid,
245 and butyric acid response ratio against acetic acid-d4.

246

247 *Statistical analysis*

248 Data are presented as the means ± SDs. Analysis was performed by using independent-sample
249 t-test on GraphPad Prism 9.0 (GraphPad Software, CA, USA), unless specified. A *p-value* of <0.05
250 was considered statistically significant. Heatmap visualization was realized using the R package
251 heatmap v1.0.12 and other figures were generated using the R package ggplot2 v3.3.5.

252

253 **Results**

254 *Body weight and feed intake were unaffected by ZEA*

255 We found that the administration of ZEA was well tolerated by the mice with a steady increase
256 in body weight (Suppl. Fig. 1A) and no evidence of reduced motor function. There was no
257 significant difference in the weight of the major organs including liver, spleen, lungs, heart and
258 kidney (Suppl. Fig. 1C) among the treatment groups. Interestingly, the body weight of the ZEA
259 group peaked after 24 days of treatment and dropped thereafter; it is anticipated that the increase
260 in tumor burden affected them. To determine whether the drop in body weight was due to a

261 potential reduced feed consumption, we analyzed the food intake throughout the treatment period.
262 The result revealed no significant difference in the feed consumption (Suppl. Fig. 1B). In
263 summary, these results indicated that body weight and feed intake were unaffected by the ZEA
264 intervention.

265

266 *ZEA promoted tumor growth*

267 We identified nearly linear increases in the tumor burden of the control (vehicle) and ZEA
268 groups over time (Fig. 1B). The tumor volume was significantly larger than that of the control (p
269 < 0.001) at the end of the intervention (Fig. 1B). The weight of the tumor in the ZEA group tripled
270 significantly ($p = 0.036$ with independent sample t-test) compared with the control group (Fig.
271 1C). The TUNEL assay showed the inhibition of tumor apoptosis by ZEA compared with the
272 control (Fig. 1D-F). Consistently, IHC staining showed that Ki67 positive cells in tumor tissues
273 were significantly increased two-fold ($p = 0.002$ with independent sample t-test) in the ZEA group
274 compared with the control (Fig. 1D-F). Together, we showed that ZEA reduced cancer cell death
275 and promoted tumor cell proliferation.

276

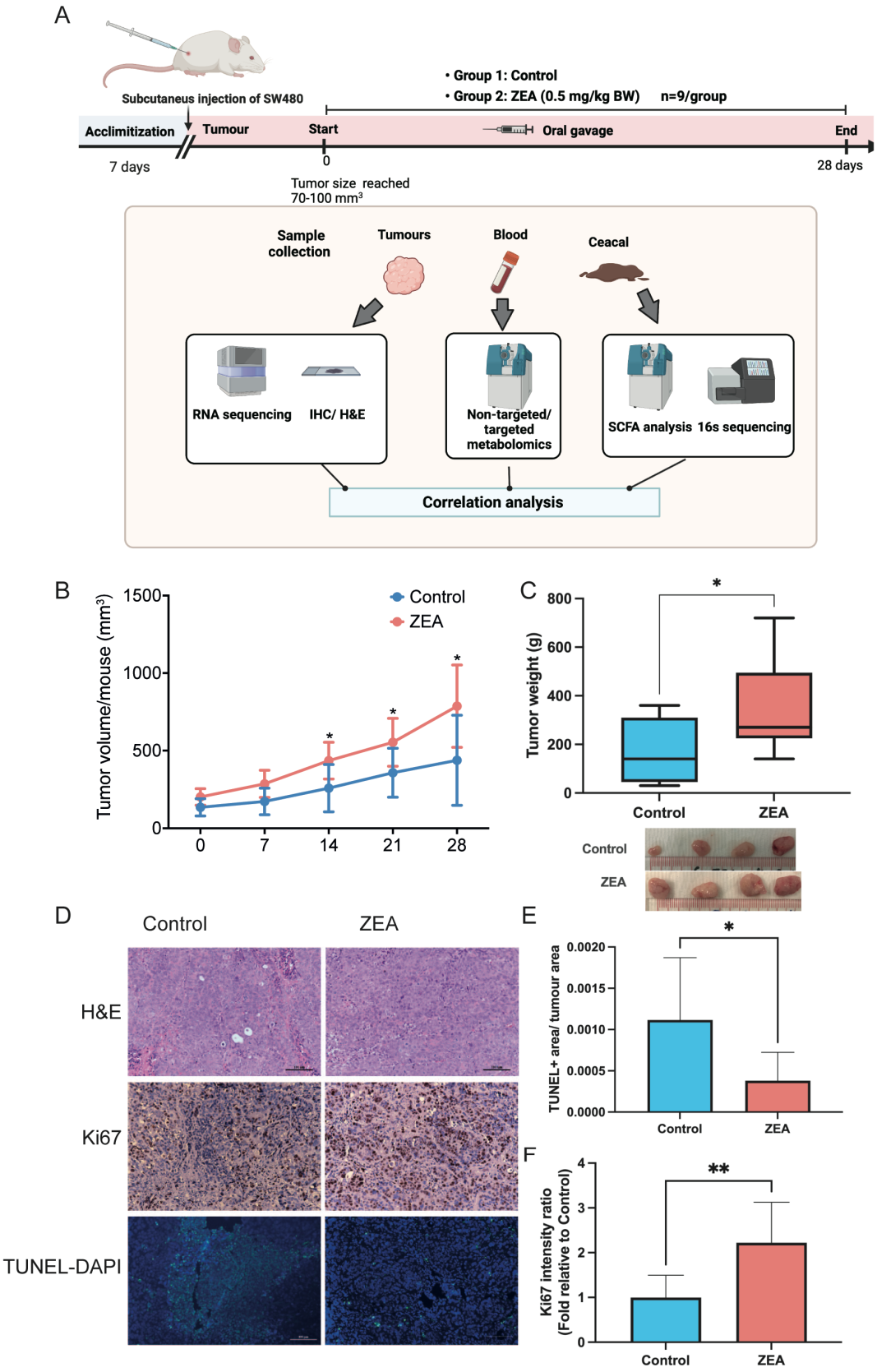
A
Subcutaneus injection of SW480
• Group 1: Control
• Group 2: ZEA (0.5 mg/kg BW) n=9/group
Acclimitization
Tumour
Start
Oral gavage
End
7 days
0
28 days
Tumor size reached
70-100 mm³
Sample collection
Tumours
Blood
Ceacal
RNA sequencing
IHC/ H&E
Non-targeted/ targeted metabolomics
SCFA analysis
16s sequencing
Correlation analysis
B
Tumor volume/mouse (mm³)
Control
ZEA
C
Tumor weight (g)
Control
ZEA
D
Control
ZEA
H&E
Ki67
TUNEL-DAPI
E
TUNEL+ area/ tumour area
F
Ki67 intensity ratio
(Fold relative to Control)

277

Fig. 1. ZEA accelerated tumor growth in a colon cancer xenograft mouse model. (A) Study design. Male 6-week-old Balb/c nude mice (n=9) were treated with vehicle (olive oil) or ZEA (0.5 mg/kg BW) thrice per week after subcutaneous injection of the human colon cancer cell line SW480. (B) Tumor volume variation during 28 days of monitoring, n=9. (C) Weight of tumors on day 28 and representative photograph of excised tumors imaged after ZEA treatment. (D) Representative microscopic photographs of H&E staining, Ki67 IHC staining, TUNEL staining (200x). (E) Quantification of TUNEL labelling was quantified as the total pixel area of the tumor. (F) while the expression of Ki67 was quantified as the relative Ki67-positive nuclei compared to the control. Signal normalized to the total pixels of the tumor (n=6-7). * $p<0.05$, ** $p<0.01$, compared to control.

Changes in gene expression associated with ZEA-induced tumor growth

DESeq2 identified 12 significantly up-regulated genes and 9 down-regulated genes (Table 1 and Fig. 2A) in the ZEA group compared with the control. According to the overall expression profile across different samples, these differentially expressed genes (DEGs) can be grouped into 3 clusters (Suppl. Fig. 2). Cluster 3 contains most of the significantly up-regulated genes, such as DGKB, EBF2, PTGIR, and BEST4. A over 20-fold expression increase ($\log_2$ fold change = 4.37) was observed in the DGKB gene (Table 1), which was previously reported as one of the gene signatures in the prognostic prediction of CRC [29]. In addition, another up-regulated gene worth mentioning is BEST4, which was previously described to be overexpressed in CRC patients [30].

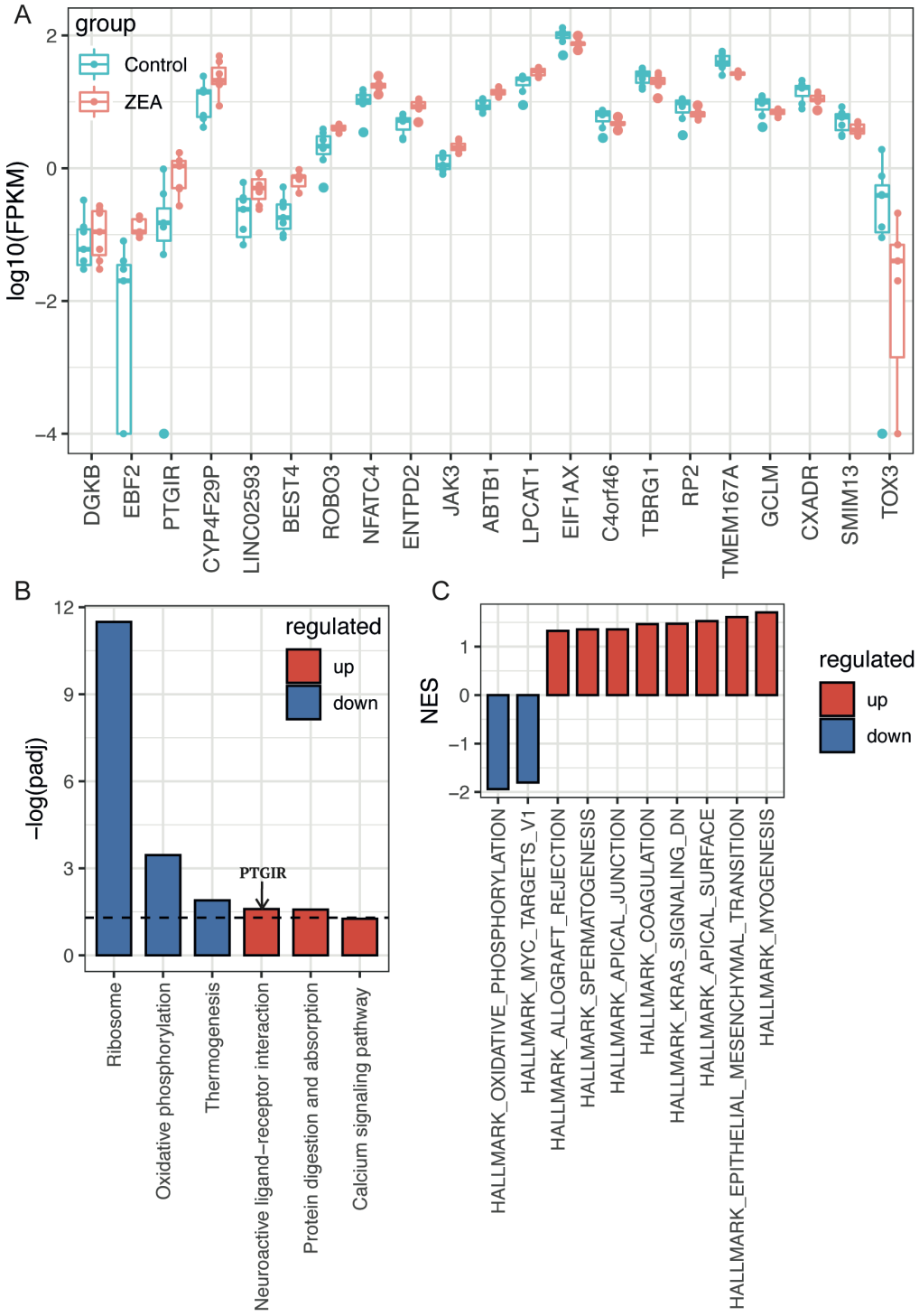

Fig. 2. Transcriptional changes in tumor cells in response to ZEA treatment. (A) Boxplot of log-transformed expression levels (in the form of FPKM values) of all differentially expressed genes identified by DESeq2 at adjusted *p-value* <0.1; (B) The histogram represents KEGG pathway enrichment result for tumor sample DEmRNAs in ZEA group compared with the control. The DE gene PTGIR was found to be involved in neuroactive ligand-receptor interaction pathways; (C)

305 Normalized enrichment scores (NES) of the positively and negatively enriched gene sets
306 (FDR < 0.25) from Molecular Signatures Database (MSigDB) hallmark gene sets significantly
307 enriched in ZEA treated mice compared to control mice.

308

309 **Table 1.** The 21 differentially expressed genes (adjusted *p-value*, a positive/negative $\log_2$ fold
310 change ($\log_2$FC) value indicates up-regulation/down-regulation) for the comparison of the ZEA
311 treatment versus the control, ranked by the $\log_2$FC.

Gene symbol	Gene name	Log_2 fold change	Adjusted *p-value*
DGKB	diacylglycerol kinase beta	4.37	0.039
EBF2	EBF transcription factor 2	2.92	0.054
PTGIR	prostaglandin I2 receptor	1.71	0.066
CYP4F29P	cytochrome P450 family 4 subfamily F member 29, pseudogene	1.37	0.013
LINC02593	long intergenic non-protein coding RNA 2593	1.36	0.054
BEST4	bestrophin 4	1.32	0.054
ROBO3	roundabout guidance receptor 3	0.84	0.022
NFATC4	nuclear factor of activated T cells 4	0.67	0.044
ENTPD2	ectonucleoside triphosphate diphosphohydrolase 2	0.63	0.054
JAK3	Janus kinase 3	0.63	0.045
ABTB1	ankyrin repeat and BTB domain containing 1	0.52	0.041
LPCAT1	lysophosphatidylcholine acyltransferase 1	0.38	0.005
TOX3	TOX high mobility group box family member 3	-3.00	0.045
SMIM13	small integral membrane protein 13	-0.56	0.018
CXADR	CXADR Ig-like cell adhesion molecule	-0.46	0.066
GCLM	glutamate-cysteine ligase modifier subunit	-0.45	0.027
TMEM167A	transmembrane protein 167A	-0.43	0.013
RP2	RP2 activator of ARL3 GTPase	-0.41	0.068
TBRG1	transforming growth factor beta regulator 1	-0.40	0.094
C4orf46	chromosome 4 open reading frame 46	-0.39	0.041
EIF1AX	eukaryotic translation initiation factor 1A X-linked	-0.34	0.025

312

313 We then performed an enrichment analysis for KEGG pathways and MSigDB gene sets,
314 including (1) cancer hallmarks, (2) oncogenic signatures and (3) chemical and genetic
315 perturbations. The result revealed three up-regulated KEGG pathways (Fig. 2B), including the
316 calcium signaling pathway (p_{adj} = 0.055), protein digestion and absorption (p_{adj} = 0.026) and
317 neuroactive ligand-receptor interaction (p_{adj}=0.025). Down-regulated pathways included ribosome

318 (p_{adj} =3.20 x 10^{-12}), oxidative phosphorylation (p_{adj} = 3.51 x 10^{-4}) and thermogenesis (p_{adj} = 0.0128)
319 (Fig. 2B). Recent studies reported that the KEGG pathway "ribosome" (ko03010) was
320 downregulated in colon cancer [31, 32]. Furthermore, the DE gene PTGIR was involved in the DE
321 up-regulated pathway neuroactive ligand-receptor interaction. Regarding the MSigDB gene sets,
322 the enrichment analysis showed that ZEA intervention promoted gene signatures representing
323 oncogenic signalling, tumor invasiveness and metastasis, such as epithelial mesenchymal
324 transition (EMT), gain of stemness, KRAS pathway and cancer invasive signature (|NES score| >
325 1 and FDR < 0.25, Fig. 2C and Suppl. Fig. 3).

326

327 *Changes in serum metabolic profiles*

328 To explore the potential metabolic consequences of the ZEA intervention, both targeted and
329 non-targeted metabolomics analyses of serum samples were performed. Overall, the metabolic
330 profiles of the ZEA intervention and control groups were separated into two clusters (Fig. 3A-B,
331 Suppl. Fig. 4A-B). A total of 41 targeted metabolites were detected, among which 19 metabolites
332 were significantly different ($p < 0.05$ with independent sample t-test) between the ZEA and control
333 groups (Fig. 3A, Suppl. Fig. 4A, Suppl. Table 1). The concentration of serum amino acid (AA)
334 was lower in the ZEA intervention group than in the control group, which was consistent with two
335 previous studies in healthy rat and porcine intestinal cell lines [33, 34]. Among the AA metabolites
336 surveyed, phosphoethanolamine, taurine, 1-methyl histidine and kynurenine had the most obvious
337 changes (|log2FC| > 0.8). In addition, a total of 21 metabolites were identified with significant
338 differences ($p < 0.05$ with independent sample t-test) between the ZEA and control groups (Fig.
339 3B, Suppl. Table 2). Fourteen of them were upregulated, including organic acids and derivatives,
340 indolic compounds, purine derivatives, and ethanolamine, etc., whereas the remaining were

341 downregulated, mainly belonging to lipids and quinazoline. Among the identified metabolites,
342 coumarinic acid, uric acid and malic acid showed the largest fold changes ($|\log_2 FC|>1$).

343 To investigate the significantly altered metabolic pathways, the log2FC of each metabolite was
344 calculated using Ingenuity Pathway Analysis for canonical pathway analysis. The top 20 canonical
345 pathways were identified and ranked according to their FDRs (Bonferroni corrected *p-values*) (Fig.
346 3C). Among these pathways, 4 activated pathways, including tRNA charging, superpathway of
347 citrulline metabolism, citrulline biosynthesis and purine nucleotides de novo biosynthesis II
348 pathway, were identified with positive z-scores in the ZEA treatment group compared with the
349 control group. The enriched citrulline metabolism and biosynthesis pathways indicated that the
350 ZEA intervention influenced the amino acid metabolism in mice, consistent with one previous
351 study using a breast cancer cell line [35].

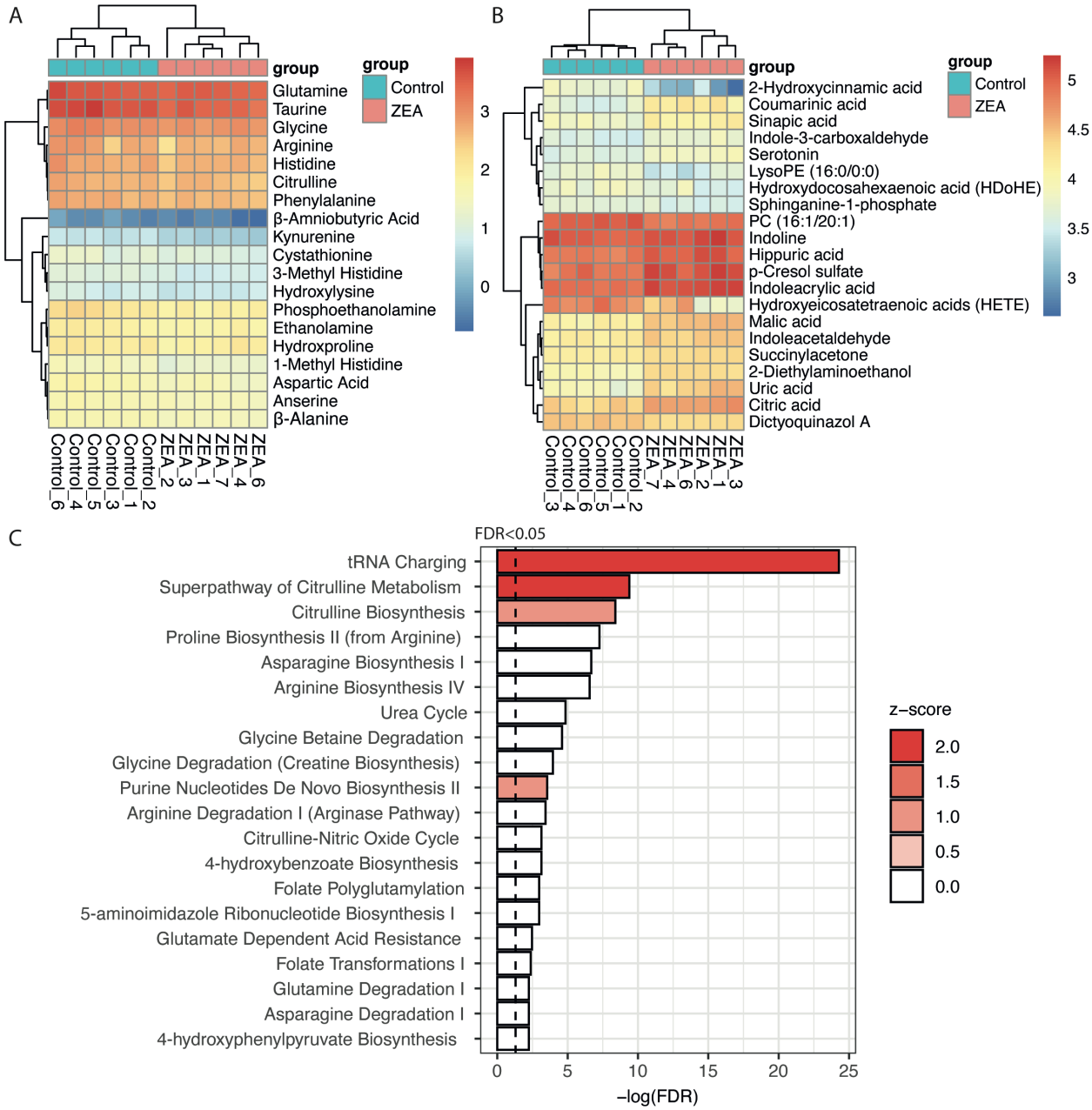

Fig. 3. Effect of ZEA intervention on metabolites in serum samples. (A) Heatmap with log-transformed levels of 19 differentially abundant metabolites between the ZEA and control groups following targeted metabolomics analysis. (B) Heatmap with log-transformed expression levels of 21 identified differentially abundant metabolites between the ZEA and control groups following non-targeted metabolomics profiling. (C) Top 20 canonical pathways identified with the -log(FDR) and z-score listed. The threshold was set at 1.3 for -log(FDR) (equivalent to FDR < 0.05).

360 *Changes in gut microbiota and microbiota-derived SCFAs*

361 The alpha diversity (Shannon index) of the gut microbiota was estimated based on the
362 taxonomic profile at the OTU level. The result indicated a significantly lower (p = 0.007 with
363 independent-sample t-test) alpha diversity in the ZEA treatment group than in the control group
364 (Fig. 4A). Moreover, multiple dimension scale (MDS) ordination based on beta diversity (robust
365 Aitchison distance) showed a difference between the two groups to a certain extent (R = 0.1254,
366 p = 0.096 with ANOSIM) (Fig. 4B). The Aitchison distances between samples in the ZEA treated
367 group were significantly larger than those in the control group (p = 0.006 with Wilcoxon test),
368 which suggests that the microbial communities became more diversified with the ZEA
369 intervention. Nine genera were significantly differentially abundant (DA) between ZEA treatment
370 and control groups based on ANCOM-BC (Fig. 4C). The relative abundances of *Alistipes,*
371 *Candidatus Saccharimonas, Helicobacter, Lachnospiraceae UCG-010, Paludicola, Rikenella,*
372 *Rikenellaceae RC9 gut group* and *Tuzzerella* were significantly lower in the ZEA treatment group
373 than in the control group (Fig. 4C, Suppl. Fig. 5). Among the differentially abundant genera,
374 *Rikenella* is an SCFA producer and *Candidatus Saccharimonas* is related to anti-inflammation
375 [36]. Together, these results suggested that ZEA possibly contributed to tumor growth through
376 repressing the SCFA-producing bacteria or anti-inflammatory bacteria.

377 We further assessed the impact of ZEA treatment on the major gut microbiota-derived SCFAs
378 (acetic acid, propionic acid, isobutyric acid, butyric acid and valeric acid) by GC-MS. Overall,
379 ZEA treatment reduced the SCFA production compared to that in the control group (Suppl. Fig.
380 6). The concentrations of total SCFAs, acetic acid, propionic acid, and butyric acid in the ZEA
381 treatment group were significantly reduced (p <0.05 with independent-sample t-test) compared to
382 the control (Suppl. Fig. 6).

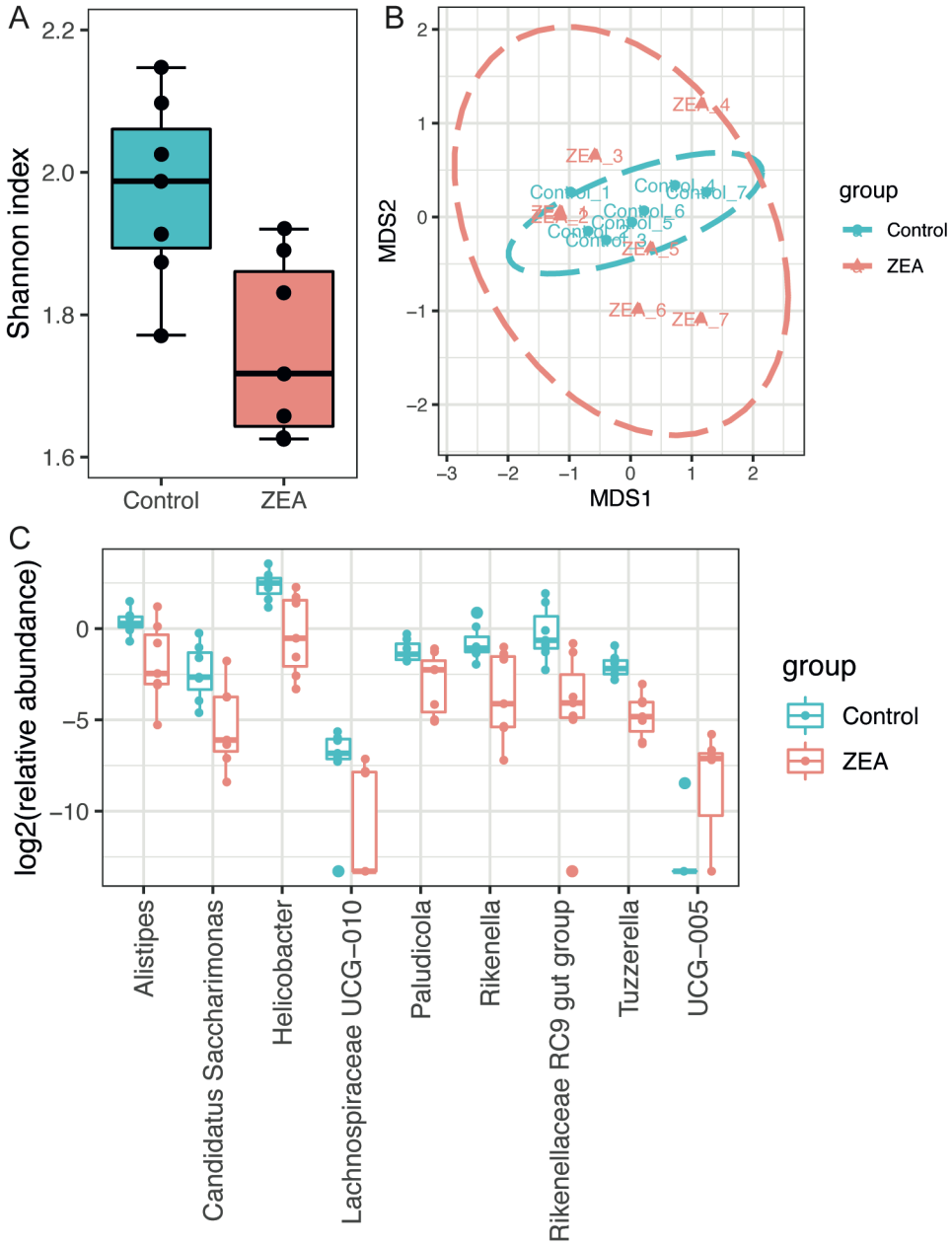

Fig. 4. Altered caecal microbiome community upon ZEA treatment. (A) Boxplot of alpha-diversity indices. Shannon index represent the community diversity of the microbiota in the caecal content. Boxes represent the interquartile range (IQR) between the first and third quartiles (25th and 75th percentiles, respectively), and the horizontal line inside the box defines the median. ** $p < 0.01$ ($p = 0.007$, independent-sample t-test). (B) Multiple dimension scale (MDS) plots showing the beta diversity results of caecal microbial profiles between the control and ZEA groups based on robust Aitchison distance. (ANOSIM statistic R 0.1254, $p = 0.096$, based on 999 permutations). (C) Boxplot of log-transformed relative abundance of significantly (FDR <0.05) different genera between the control and ZEA detected by ANCOM-BC.

394 *Associations among gene expression, metabolites and gut microbes*

395 A total of 13 metabolites were significantly correlated with tumor weight using Spearman's
396 correlation (Suppl. Table 3). Among them, six identified metabolites, including indolic compounds
397 and derivatives (serotonin and indoleacetaldehyde), purine derivatives (uric acid), and organic
398 acids derivatives (p-cresol sulfate, succinylacetone and hippuric acid), were positively correlated
399 with tumor weight (correlation > 0.6, $p < 0.05$). In contrast, other metabolites, including two amino
400 acids (1-methyl histidine and β-alanine) and lipid-related molecules (HDoHE and HETE), etc,.
401 were negatively correlated (correlation < -0.6, $p < 0.05$) with tumor weight.

402 To establish links among differentially expressed genes, differentially abundant metabolites
403 and differentially abundant gut microbes, Spearman's correlation coefficients were calculated. A
404 total of 12 significantly and strongly (FDR < 0.05 and |correlation|>0.8) positive and 21
405 significantly and strongly negative correlations were identified for integration analysis (Fig. 5 A,
406 Suppl. Table 4). These 33 associations consisted of 36 features (12 differentially expressed genes,
407 19 differentially abundant metabolites and five differentially abundant genera) (Fig. 5 A & B).
408 Majority (25 out 33, 75.8%) of the assocations are between metabolites and genes expression.
409 Among the 19 differentially abundant metabolites, ten metabolites were significantly correlated
410 with tumor weight. More specifically, indolic compounds and derivatives (serotonin and
411 indoleacetaldehyde), purine derivatives (uric acid), and organic acids derivatives (p-cresol sulfate,
412 succinylacetone, hippuric acid and 2-hydroxycinnamic acid), were positively correlated with
413 tumor weight, while two amino acids (1-methyl histidine and β-alanine) and one lipid-related
414 molecule (HETE) were negatively correlated with tumor weight. Our results revealed strong
415 connections between host metabolism and the metabolic potential of the gut microbes.

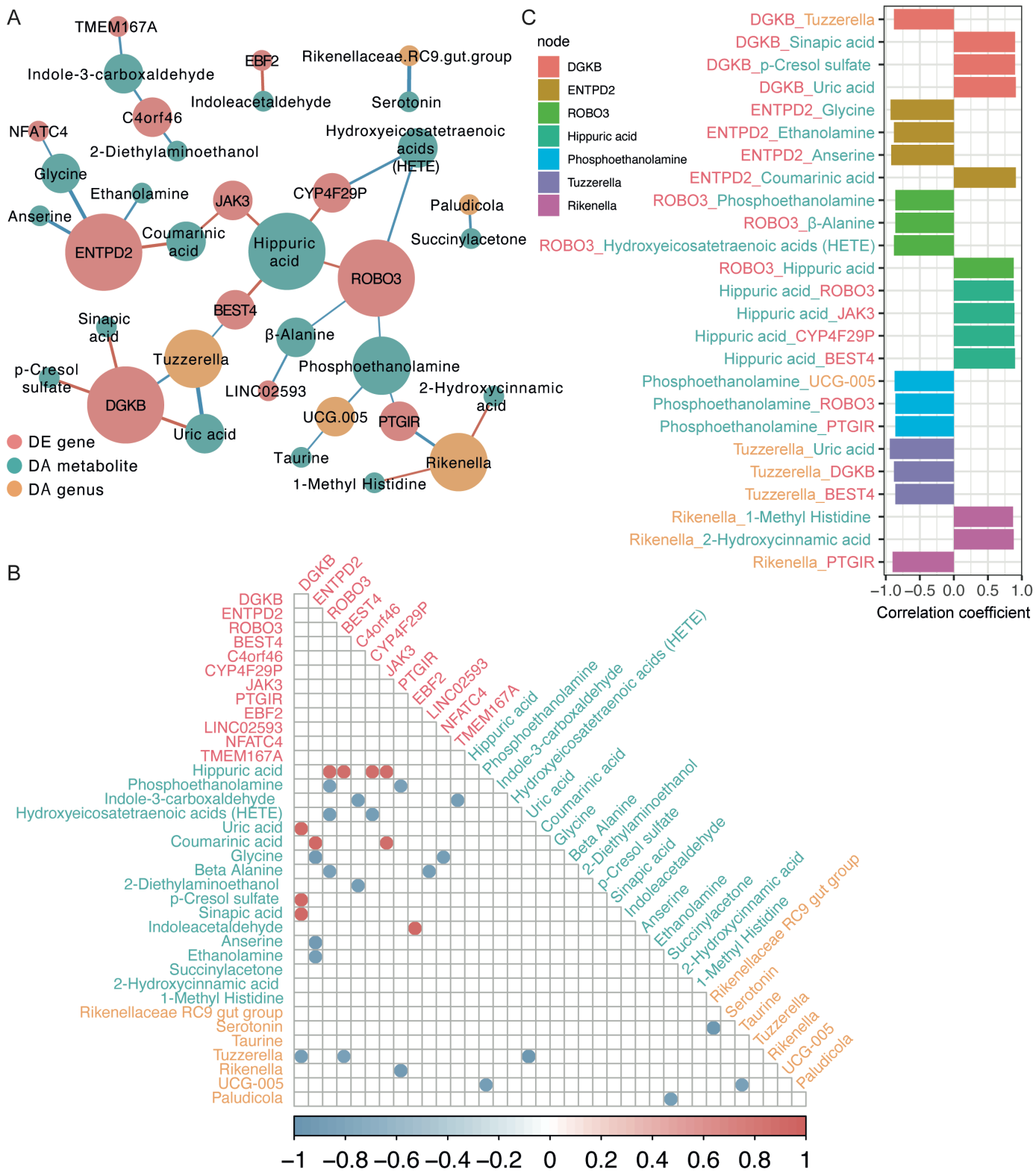

Fig. 5. Integrative analysis of the differentially expressed genes, differentially abundant genera, and differentially abundant metabolites using Pearson correlation. (A) Association network

showing the Pearson correlation analysis of differentially expressed genes (red nodes), differentially abundant genera (orange nodes), and differentially abundant metabolites (dark green nodes). The significant correlations (Bonferroni corrected FDR<0.05) are shown in the network. Red lines represent positive correlations, and blue lines represent negative correlations; (B) Corrplot depicting the correlations among differentially expressed genes, differentially abundant genera and differentially abundant metabolites. Only features showing the correlations of > 0.8 or < −0.8 in any of the pairwise associations were included for visualization. The significance level was set at an FDR < 0.05; (C) Boxplot showing correlation of seven nodes whose degree ≥ 3 in Fig. 5(A). DGKB, diacylglycerol kinase beta; ENTPD2, ectonucleoside triphosphate diphosphohydrolase 2; ROBO3, roundabout guidance receptor 3; Hippuric acid; Phosphoethanolamine; *Tuzzerella*; *Rikenella*.

Seven nodes had at least three associations with other features (Fig. 5A & C). Among these nodes, the differentially expressed gene DGKB was strongly (|correlation|>0.8) positively correlated with uric acid (correlation = 0.909), p-Cresol sulfate (correlation = 0.902) and sinapic acid (correlation = 0.902), negatively correlated with *Tuzzerella* (correlation = -0.881) (Fig. 5 A-C), indicating that the interplay among host metabolites, gut microbiota and tumor gene expression may contribute to the ZEA-induced tumor growth. Among the metabolite features, hippuric acid was frequently associated with multiple differentially expressed genes with oncogenic potential (positive correlation with BEST4 (correlation = 0.895), CYP4F29P (correlation = 0.888), JAK3 (correlation = 0.888) and ROBO3 (correlation = 0.881)) (Fig. 5 A-C). Additionally, *Tuzzerella* showed the largest number of associations with other genes/metabolites. *Tuzzerella* were negatively associated with BEST4 (correlation = -0.86), DGKB (correlation = -0.881) and uric acid (correlation = -0.937) (Fig. 5 A-C). In summary, these identified gene-metabolite-genus crosslinks provide a mechanistic insight into the zearalenone-aggravated tumor growth in CRC.

445 **Discussion**

446 In the present study, we performed a comprehensive and integrative multi-omics study to
447 unveil the underlying molecular mechanisms of the effect of ZEA on CRC. Through an integrative
448 multi-omics analysis, we revealed that ZEA promoted CRC tumor growth through promoting
449 BEST4/AKT/ERK1/2 pathway, modifying serum metabolites and modulating gut microbiota
450 composition.

451 Among the 21 differentially expressed genes in the tumor section, two ZEA-promoted genes
452 (bestrophin 4, BEST4; diacylglycerol kinase beta, DGKB) in the ZEA group were reported to be
453 related to the malignant growth of colon cancer. BEST4 was found to be upregulated in CRC
454 patients, and its high expression was correlated with a more advanced TNM stage, lymph node
455 metastasis and worse survival rate by activating the BEST4/PI3K/AKT signaling pathway [30].
456 Our further RT–PCR analysis confirmed that BEST4 was significantly up-regulated in the ZEA
457 group (p = 0.024 with independent-sample t-test) (Suppl. Fig. 7). IHC staining showed increased
458 protein levels of BEST4 and DGBK (Suppl. Fig. 8A-B). In the following IHC staining, we
459 confirmed that the levels of phosphorylated ERK1/2 and AKT were significantly increased (Suppl.
460 Fig. 8A-B). We found an up-regulated BEST4 level which could contribute to the activation of
461 AKT and ERK1/2, consistent with He et al. study [30]. DGKB was previously found to be one of
462 the gene signatures of prognostic prediction in CRC [29]. However, the exact role of DGKB in
463 colon cancer pathology is still unclear.

464 Through KEGG pathway enrichment analysis, we found a strong suppression in the
465 "ribosome" (KEGG pathway 03010). Although pathway ribosome was previously linked to cancer
466 progression through providing metabolic needs to the actively growing cancer cells, recent studies
467 from five independent datasets have shown that ribosome biogenesis was one of the downregulated

468 KEGG pathways in colon cancer [31, 32]. Furthermore, it is known that cancer promotes the shift
469 from an aerobic to anaerobic metabolic pathway to survive the highly hypoxic nature of a
470 hyperproliferating tumor. Our findings showed that ZEA downregulated the oxidative
471 phosphorylation pathway while enriching protein digestion and absorption. The suppression in
472 oxidative phosphorylation is consistent with a lower level of TCA metabolites, such as malic acid
473 and citric acid (Suppl. Fig. 4), in serum.

474 We conducted non-targeted and targeted metabolomics analyses of serum samples to reveal
475 the metabolic influence of the ZEA intervention. We found that the serum amino acid (AA)
476 concentration was lower in the ZEA-treated group (Suppl. Table 1-2). The finding is in line with
477 previous findings in healthy rat and porcine intestinal cell lines, in which ZEA altered amino acid
478 metabolism [33, 34]. Cancer cells proliferate at a higher rate than healthy cells; hence their
479 metabolic demand is larger. Amino acid is a class of essential nutrients for healthy cells, and
480 plasma amino acid concentrations were previously found to be generally lower in lung, gastric,
481 colorectal, breast, or prostate cancer patients [37-39]. Patients with a more advanced stages of
482 CRC were found to have a lower circulatory citrulline, histidine and glutamine levels [39, 40].
483 Indeed, a lower serum histidine, 1-methyl histidine, 3-methyl histidine, citrulline and glutamine
484 levels, and enrichment in the citrulline metabolism and biosynthesis pathways in the ZEA group
485 were observed. A negative correlation between tumor weight and histidine derivative, 1-methyl
486 histidine, were found in our study. Such a reduction of histidine is suggested to be connected to
487 the increased histidine decarboxylate activity which was found to be correlated with tumor stages
488 as histidine could act as an angiogenic factor [41, 42]. In addition, we found a strong negative
489 correlation between β-alanine and tumor weight, which was consistent with the findings from Bi
490 et al. β-alanine was reported to have a negative correlation with the tumor invasiveness score, a

491 measurement of tumor angiogenesis [43]. On the other hand, glycine was reported as a biomarker
492 for colon cancer whose levels were significantly lower in CRC patients than in healthy individuals
493 [44]. In agreement with the finding from Leichtle et al., we found a significantly lower serum
494 glycine level in the ZEA group. Overall, serum amino acid profile supports the enrichment protein
495 digestion and absorption in KEGG pathway of our transcriptome analysis, as the circulatory amino
496 acid abundancy drop.

497 Non-targeted inflammation-related metabolites were also significantly altered in the ZEA
498 group. We found that serum uric acid had the second highest fold change among the detected
499 untargeted metabolites when compared with the control group, suggesting the role of ZEA in
500 altering purine metabolism. High serum uric acid was indicated to promote inflammation and
501 contribute to the increased tumor cell proliferation [45], while the decline in glutamine was found
502 to be an indicator of systemic inflammation in CRC patients [40]. Apart from amino acids,
503 concentrations of lipid-related metabolites were also lower in the ZEA group (Fig. 3B) and
504 negatively correlated with tumor weight (Suppl. Table 3). We observed that serum
505 hydroxyeicosatetraenoic acids (HETE) level was lower in the ZEA group, potentially leading to
506 defects in PPARγ activation which is responsible for apoptosis in CRC [46]. Another lipid-related
507 metabolite, hydroxydocosahexaenoic acid (HDoHE), was also found to be negatively correlated
508 with tumor weight, in line with a previous study that revealed that a higher level of HDoHE was
509 associated with smaller CRC tumors in mice due to the anti-inflammatory property of HDoHE
510 [47]. These results suggested that ZEA could possibly hinder the production of anti-inflammatory
511 metabolites, leading to aggravated tumor growth.

512 It is well known that the gut microbiota plays an important role in regulating the host's immune
513 system. Alteration of the microbial community is known to influence the development of diseases,

514 such as irritable bowel disease, obesity, liver disease and cancer [48-50]. In our study, the
515 abundances of SCFA-producing bacteria, including *Rikenella* [51] and *Rikenellaceae RC9 gut*
516 *group*, and the anti-inflammatory bacteria *Candidatus Saccharimonas* [36] were lowered in the
517 ZEA-treated mice. The suppression of SCFA producing bacteria was confirmed with the decreased
518 caecal SCFAs concentration in our study. Our finding is consistent with a previous study that
519 revealed a significantly lower caecal SCFAs content in the ZEA-treated animal group [52]. Low
520 abundance of SCFAs, major metabolites from gut microbiota, and SCFAs-producing bacteria are
521 linked to colon cancer development [53].

522 We further conducted an integrative analysis of multi-omics data, including differentially
523 expressed genes, differentially abundant metabolites and differentially abundant genera. The
524 results revealed that the abundance of *Tuzzerella* is negatively correlated with serum uric acid level
525 which was previously reported to activate PI3K/AKT pathway [54]. Subsequently, the lower
526 abundance of *Tuzzerella* in the ZEA group could lead to tumor cell proliferation and PI3K/AKT
527 activation due to the increased level of uric acid. However, the role of *Tuzzerella* in tumor
528 pathogenesis is still unclear; thus, further study is needed to uncover its metabolic influence and
529 interactions with uric acid secretion. In addition, the abundance of *Tuzzerella* is negatively
530 correlated with the expression of BEST4 which could bind to PI3K and activate AKT. Further
531 studies are warranted to confirm and explain such correlations.

532 Apart from uric acid, 10 other differentially abundant serum metabolites, which were strongly
533 correlated with tumor weight, were also found to be strongly associated with the differentially
534 expressed genes or differentially abundant genera in our integrative analysis. Similar to uric acid,
535 p-cresol sulfate was found to be positively correlated with the DGKB gene, which was reported to
536 be associated with CRC malignant growth [29]. In this study, we observed a significantly higher

537 serum level of p-cresol sulfate in the ZEA group. P-cresol sulfate was reported to induce
538 inflammation and tumor growth in colon cancer [55]. In addition, p-cresol sulfate is derived from
539 microbial metabolism and conjugation in the colon from amino acids, phenylalanine and tyrosine
540 [56]. This also explains the significantly lower phenylalanine levels in the ZEA group as
541 phenylalanine could be metabolized or converted to tyrosine following microbial conversion.
542 Moreover, among the identified serum metabolites, hippuric acid was significantly positively
543 correlated with BEST4, JAK3, ROBO3 and CYP4F29P genes. In particular, BEST4, JAK3 and
544 ROBO3 were reported to promote tumor cell proliferation through activating different signaling
545 pathways, including the PI3K/AKT, JAK3/STAT3 and SLIT/ROBO pathways, respectively [30,
546 57, 58]. These results suggested that hippuric acid played a role in promoting tumor growth upon
547 ZEA treatment through alteration of oncogenic gene expression. It is also worth noting that the
548 serum level of hippuric was elevated upon ZEA treatment. The production of hippuric acid
549 involves the conjugation of glycine to benzoic acid [59]. Alternatively, it may also be formed from
550 the gut microbiota metabolism of phenylalanine [60]. These results possibly explain the significant
551 reduction of the amino acid glycine and phenylalanine but elevated hippuric acid levels in the ZEA
552 group. Furthermore, several indolic compounds were also significantly altered and were strongly
553 associated with several differentially expressed genes in this study. Collectively, we showed that
554 ZEA played an important part in altering gut microbiota, microbiota-derived metabolites and
555 oncogenic gene expression during CRC progression.

556 By establishing a patient-derived xenograft CRC mouse model, we provided novel and
557 comprehensive mechanistic insights into how ZEA promoted tumor development in CRC using
558 integrative multi-omics approaches. However, there are several limitations in the current study.
559 One major limitation of this study is that an animal model used here may not inform the same

560 human responses under ZEA intervention. Although human and mouse share similar physiology
561 and anatomy structure, only 15% of gut commensal bacteria are shared between mice and human.
562 Most human microbiome studies utilized faecal samples as human ferment indigestible food
563 components in the colon, while cecum is the site of fermentation in mouse [61]. This may lead to
564 discrepancies when translating to a clinical setting. Additionally, we were unable to distinguish
565 bacterial species and identify the metabolic features of the microbiome due to the limitation of the
566 16S rDNA sequencing. To more accurately estimate effect of ZEA on human subjects with CRC,
567 we suggested a humanized mouse model with shotgun metagenomic sequencing in the future.
568 Another limitation will be the small sample size with only nine mice per group, which could limit
569 the power of the study.

570

571 **Conclusions**

572 In summary, this study provided evidence that ZEA could promote tumor growth and
573 development in colon cancer. We demonstrated that an exposure to ZEA resulted in altered tumor
574 transcriptome, serum metabolome and gut microbiota. ZEA-induced tumor promotion is likely
575 through modulating the BEST4/AKT/ERK1/2 pathway, reducing circulatory amino acid, and
576 altering microbiota composition. Through integration and correlation analysis of multi-omics data,
577 we found that the genus *Tuzzerella* was significantly negatively correlated with the BEST4
578 expression level and the serum metabolite, uric acid, which was positively correlated with tumor
579 weight. The circulatory hippuric acid level was found to be significantly positively associated with
580 the tumor weight and the expression levels of oncogenic genes, such as BEST4, indicating its
581 contribution to the observed tumor growth. Since ZEA is commonly found in the human diet and

its impact can be persistent, further studies on the potential contribution of chronic exposure of ZEA to colon cancer development are warranted.

Compliance with Ethics Requirement

All Institutional Guidelines for the care and use of animals were followed. Animal handling for the experimentation was approved by the Committee on the Use of Live Animals in Teaching and Research (CULATR No. 4785-18), the University of Hong Kong.

CRediT authorship contribution statement

Conceptualization, E.K.K.L. and H.E.; methodology, E.K.K.L., X.W.W, P.K.L., H.W.; investigation, E.K.K.L., X.W.W., P.K.L., H.C.W., D.Z., J.L. and H.E.; writing - original draft, E.K.K.L., X.W.W, writing - review and editing E.K.K.L., X.W.W., P.K.L, J.C.Y.L, C.G.G., D.Z, J.L. and H.E.; funding acquisition, D.Z, J.L. and H.E. All authors have read and agreed to the published version of the manuscript.

Data Availability Statement

Transcriptome and 16S rDNA data were archived in the National Center for Biotechnology Information (NCBI) Short Read Archive (SRA): PRJNA875586.

Declaration of Competing Interest

The authors declare that they have no known competing financial interests or personal relationships that could have appeared to influence the work reported in this paper.

Acknowledgments

The authors especially thanks Mr. Oscar Chow for providing technical assistance. The authors are grateful to Dr. Sam Leung Kin Sum for creating the preliminary data on SCFAs. This study was supported by Shenzhen Basic Research Program (JCYJ20190808182402941), Guangdong Basic and Applied Research Major Program (2019B030302005), Collaborative Research Fund (C7013-19GF) in Hong Kong and City University of Hong Kong internal grant (7005530, 7005756, 9678247, 9680310), and PolyU Start-up fund (1-BE3H).

Supplementary material

Supplementary data to this article can be found at https://doi.org/xxxx. Supplementary figure 1: Effect of Zearalenone in body weight, feed consumption and vital organ weight of xenograft mice; Supplementary figure 2: Heatmap of log-transformed expression levels (in the form of FPKM values) of all differentially expressed genes identified by DESeq2 at padj <0.1; Supplementary figure 3: Correlations between ZEA treatment and potential oncogenic signaling; Supplementary figure 4: Effect of ZEA treatment on metabolites in serum samples; Supplementary figure 5: Heatmap of log-transformed relative abundance of significantly (FDR <0.05) different genera between control and ZEA detected by ANCOM-BC; Supplementary figure 6: Effect on the SCFA levels in the caecal contents upon treatment; Supplementary figure 7: qPCR analysis of the mRNA expression of BEST4; Supplementary figure 8: Transcriptional changes in tumor cells in response to ZEA treatment; Supplementary Table

621 1: Amino acids that were altered by ZEA treatment compared to control group; Supplementary Table 2: List of
622 metabolites detected in serum samples of control and experimental groups using Progenesis QI; Supplementary
623 Table3: Metabolites strongly related to tumor weight with spearman's rank correlation coefficient; Supplementary
624 Table4: Pearson correlation coefficient and significance level for DA metabolites, DE genes and DA genera;
625 Supplementary methods: RNA extraction and Real time reverse transcription polymerase chain reaction (RT-qPCR).

626

627 **References**

628 1. Bray, F., et al., *Global cancer statistics 2018: GLOBOCAN estimates of incidence and mortality worldwide*
629 *for 36 cancers in 185 countries.* Ca-a Cancer Journal for Clinicians, 2018. **68**(6): p. 394-424.
630 2. Qie, Y., et al., *Environmental Estrogens and Their Biological Effects through GPER Mediated Signal*
631 *Pathways*.* Environmental Pollution, 2021. **278**.
632 3. Belhassen, H., et al., *Zearalenone and its metabolites in urine and breast cancer risk: a case-control study*
633 *in Tunisia.* Chemosphere, 2015. **128**: p. 1-6.
634 4. Yip, K.Y., et al., *Combined low-dose zearalenone and aflatoxin B1 on cell growth and cell-cycle progression*
635 *in breast cancer MCF-7 cells.* Toxicology Letters, 2017. **281**: p. 139-151.
636 5. Kowalska, K., et al., *Estrogen receptor α is crucial in zearalenone-induced invasion and migration of*
637 *prostate cancer cells.* Toxins, 2018. **10**(3): p. 98.
638 6. Abassi, H., et al., *The mycotoxin zearalenone enhances cell proliferation, colony formation and promotes*
639 *cell migration in the human colon carcinoma cell line HCT116.* Toxicol Lett, 2016. **254**: p. 1-7.
640 7. Lo, E.K.K., et al., *Low dose of zearalenone elevated colon cancer cell growth through G protein-coupled*
641 *estrogenic receptor.* Sci Rep, 2021. **11**(1): p. 7403.
642 8. Jackson, E.L. and H. Lu, *Three-dimensional models for studying development and disease: moving on from*
643 *organisms to organs-on-a-chip and organoids.* Integr Biol (Camb), 2016. **8**(6): p. 672-83.
644 9. Ma, H., et al., *Correlation between microbes and colorectal cancer: tumor apoptosis is induced by sitosterols*
645 *through promoting gut microbiota to produce short-chain fatty acids.* Apoptosis, 2019. **24**(1-2): p. 168-183.
646 10. Vipperla, K. and S.J. O'Keefe, *Diet, microbiota, and dysbiosis: a 'recipe' for colorectal cancer.* Food Funct,
647 2016. **7**(4): p. 1731-40.
648 11. Yoon, K. and N. Kim, *The Effect of Microbiota on Colon Carcinogenesis.* J Cancer Prev, 2018. **23**(3): p.
649 117-125.
650 12. Garrett, W.S., *The gut microbiota and colon cancer.* Science, 2019. **364**(6446): p. 1133-1135.
651 13. Sethi, V., et al., *Gut Microbiota Promotes Tumor Growth in Mice by Modulating Immune Response.*
652 Gastroenterology, 2018. **155**(1): p. 33-37 e6.
653 14. Tan, S., et al., *Zearalenone-induced aberration in the composition of the gut microbiome and function*
654 *impacts the ovary reserve.* Chemosphere, 2020. **244**: p. 125493.
655 15. Tan, S.J., et al., *Zearalenone-induced aberration in the composition of the gut microbiome and function*
656 *impacts the ovary reserve.* Chemosphere, 2020. **244**.
657 16. Zhang, W., et al., *Changes in intestinal barrier functions and gut microbiota in rats exposed to zearalenone.*
658 Ecotoxicology and Environmental Safety, 2020. **204**.
659 17. Zhang, W., et al., *Changes in intestinal barrier functions and gut microbiota in rats exposed to zearalenone.*
660 Ecotoxicology and Environmental Safety, 2020. **204**: p. 111072.
661 18. Pfohl-Leszkowicz, A., L. Chekir-Ghedira, and H. Bacha, *Genotoxicity of zearalenone, an estrogenic*
662 *mycotoxin: DNA adduct formation in female mouse tissues.* Carcinogenesis, 1995. **16**(10): p. 2315-20.
663 19. Nair, A.B. and S. Jacob, *A simple practice guide for dose conversion between animals and human.* J Basic
664 Clin Pharm, 2016. **7**(2): p. 27-31.
665 20. Li, F.L., et al., *Acetylation accumulates PFKFB3 in cytoplasm to promote glycolysis and protects cells from*
666 *cisplatin-induced apoptosis.* Nat Commun, 2018. **9**(1): p. 508.
667 21. Kopylova, E., L. Noé, and H. Touzet, *SortMeRNA: fast and accurate filtering of ribosomal RNAs in*
668 *metatranscriptomic data.* Bioinformatics, 2012. **28**(24): p. 3211-3217.
669 22. Zheng, T., et al., *Mining, analyzing, and integrating viral signals from metagenomic data.* Microbiome, 2019.
670 **7**(1): p. 1-15.
671 23. Fayzullina, S. and L.J. Martin, *Detection and Analysis of DNA Damage in Mouse Skeletal Muscle In Situ*
672 *Using the TUNEL Method.* Jove-Journal of Visualized Experiments, 2014(94).
673 24. Crowe, A.R. and W. Yue, *Semi-quantitative Determination of Protein Expression*
674 *UsingImmunohistochemistry Staining and Analysis: An Integrated Protocol.* Bio-protocol, 2019. **9**(24).

675 25. Van den Boogaart, K.G. and R. Tolosana-Delgado, *"Compositions": a unified R package to analyze*
676 *compositional data.* Computers & Geosciences, 2008. **34**(4): p. 320-338.
677 26. Lin, H. and S.D. Peddada, *Analysis of compositions of microbiomes with bias correction.* Nature
678 communications, 2020. **11**(1): p. 1-11.
679 27. Zheng, X., et al., *A targeted metabolomic protocol for short-chain fatty acids and branched-chain amino*
680 *acids.* Metabolomics, 2013. **9**(4): p. 818-827.
681 28. Cai, J., et al., *Orthogonal Comparison of GC-MS and (1)H NMR Spectroscopy for Short Chain Fatty Acid*
682 *Quantitation.* Anal Chem, 2017. **89**(15): p. 7900-7906.
683 29. Luo, D.K., et al., *A Novel Seventeen-Gene Metabolic Signature for Predicting Prognosis in Colon Cancer.*
684 Biomed Research International, 2020. **2020**.
685 30. He, X.S., et al., *Oncogenic potential of BEST4 in colorectal cancer via activation of PI3K/Akt signaling.*
686 Oncogene, 2022. **41**(8): p. 1166-1177.
687 31. Mastrogamvraki, N. and A. Zaravinos, *Signatures of co-deregulated genes and their transcriptional*
688 *regulators in colorectal cancer (vol 6, 23, 2020).* Npj Systems Biology and Applications, 2020. **6**(1).
689 32. Shen, A.L., et al., *EBF1-Mediated Upregulation of Ribosome Assembly Factor PNO1 Contributes to Cancer*
690 *Progression by Negatively Regulating the p53 Signaling Pathway.* Cancer Research, 2019. **79**(9): p. 2257-
691 2270.
692 33. Liu, G., et al., *Biological system responses to zearalenone mycotoxin exposure by integrated metabolomic*
693 *studies.* J Agric Food Chem, 2013. **61**(46): p. 11212-21.
694 34. Wang, H., et al., *Integrated Metabolomics and Transcriptomics Analyses Reveal Metabolic Mechanisms in*
695 *Porcine Intestinal Epithelial Cells under Zearalenone Stress.* Journal of Agricultural and Food Chemistry,
696 2022.
697 35. Nittoli, A.C., et al., *Effects of α-zearalenol on the metabolome of two breast cancer cell lines by 1H-NMR*
698 *approach.* Metabolomics, 2018. **14**(3): p. 33.
699 36. He, R., et al., *Cancer-Preventive Role of Bone Marrow-Derived Mesenchymal Stem Cells on Colitis-*
700 *Associated Colorectal Cancer: Roles of Gut Microbiota Involved.* Front Cell Dev Biol, 2021. **9**: p. 642948.
701 37. Miyagi, Y., et al., *Plasma free amino acid profiling of five types of cancer patients and its application for*
702 *early detection.* PLoS One, 2011. **6**(9): p. e24143.
703 38. Hashim, N.A.A., et al., *Global serum metabolomics profiling of colorectal cancer.* Mol Clin Oncol, 2019.
704 **11**(1): p. 3-14.
705 39. Geijsen, A.J.M.R., et al., *Plasma metabolites associated with colorectal cancer stage: Findings from an*
706 *international consortium.* International Journal of Cancer, 2020. **146**(12): p. 3256-3266.
707 40. Sirnio, P., et al., *Alterations in serum amino-acid profile in the progression of colorectal cancer: associations*
708 *with systemic inflammation, tumour stage and patient survival.* Br J Cancer, 2019. **120**(2): p. 238-246.
709 41. Di Donato, S., et al., *A Serum Metabolomics Classifier Derived from Elderly Patients with Metastatic*
710 *Colorectal Cancer Predicts Relapse in the Adjuvant Setting.* Cancers (Basel), 2021. **13**(11).
711 42. Zhu, J., et al., *Colorectal cancer detection using targeted serum metabolic profiling.* Journal of proteome
712 research, 2014. **13**(9): p. 4120-4130.
713 43. Zuazo-Gaztelu, I. and O. Casanovas, *Unraveling the Role of Angiogenesis in Cancer Ecosystems.* Front
714 Oncol, 2018. **8**: p. 248.
715 44. Leichtle, A.B., et al., *Serum amino acid profiles and their alterations in colorectal cancer.* Metabolomics,
716 2012. **8**(4): p. 643-653.
717 45. Yan, J. and C. Zhu, *Hyperuricemia is a Adverse Prognostic Factor for Colon Cancer Patients.* Int J Gen
718 Med, 2021. **14**: p. 3001-3006.
719 46. Pakiet, A., et al., *Changes in lipids composition and metabolism in colorectal cancer: a review.* Lipids Health
720 Dis, 2019. **18**(1): p. 29.
721 47. Nakanishi, M., et al., *A novel bioactive derivative of eicosapentaenoic acid (EPA) suppresses intestinal tumor*
722 *development in ApcΔ14/+ mice.* Carcinogenesis, 2018. **39**(3): p. 429-438.
723 48. Ohtani, N., S. Yoshimoto, and E. Hara, *Obesity and cancer: a gut microbial connection.* Cancer Res, 2014.
724 **74**(7): p. 1885-9.
725 49. Qin, N., et al., *Alterations of the human gut microbiome in liver cirrhosis.* Nature, 2014. **513**(7516): p. 59-
726 64.
727 50. Imhann, F., et al., *Interplay of host genetics and gut microbiota underlying the onset and clinical presentation*
728 *of inflammatory bowel disease.* Gut, 2018. **67**(1): p. 108-119.
729 51. Shi, H., et al., *Dietary fucoidan of Acaudina molpadioides alters gut microbiota and mitigates intestinal*
730 *mucosal injury induced by cyclophosphamide.* Food Funct, 2017. **8**(9): p. 3383-3393.

731 52. Cai, J., et al., *Bacillus velezensis A2 Inhibited the Cecal Inflammation Induced by Zearalenone by Regulating*
732 *Intestinal Flora and Short-Chain Fatty Acids.* Front Nutr, 2022. **9**: p. 806115.
733 53. Hou, H., et al., *Gut microbiota-derived short-chain fatty acids and colorectal cancer: Ready for clinical*
734 *translation?* Cancer Letters, 2022. **526**: p. 225-235.
735 54. Chen, M., et al., *Soluble uric acid increases PDZK1 and ABCG2 expression in human intestinal cell lines*
736 *via the TLR4-NLRP3 inflammasome and PI3K/Akt signaling pathway.* Arthritis Res Ther, 2018. **20**(1): p. 20.
737 55. Rivas-Domínguez, A., et al., *The Role of DNA Damage Response in Dysbiosis-Induced Colorectal Cancer.*
738 Cells, 2021. **10**(8).
739 56. Gryp, T., et al., *p-Cresyl Sulfate.* Toxins (Basel), 2017. **9**(2).
740 57. Zhou, W.J., et al., *Slit-Robo signaling induces malignant transformation through Hakai-mediated E-cadherin*
741 *degradation during colorectal epithelial cell carcinogenesis.* Cell Res, 2011. **21**(4): p. 609-26.
742 58. Lin, Q., et al., *Constitutive activation of JAK3/STAT3 in colon carcinoma tumors and cell lines: inhibition of*
743 *JAK3/STAT3 signaling induces apoptosis and cell cycle arrest of colon carcinoma cells.* Am J Pathol, 2005.
744 **167**(4): p. 969-80.
745 59. Pallister, T., et al., *Hippurate as a metabolomic marker of gut microbiome diversity: Modulation by diet and*
746 *relationship to metabolic syndrome.* Sci Rep, 2017. **7**(1): p. 13670.
747 60. Sarkissian, C.N., C.R. Scriver, and O.A. Mamer, *Quantitation of phenylalanine and its trans-cinnamic,*
748 *benzoic and hippuric acid metabolites in biological fluids in a single GC-MS analysis.* J Mass Spectrom,
749 2007. **42**(6): p. 811-7.
750 61. Nguyen, T.L.A., et al., *How informative is the mouse for human gut microbiota research?* Disease models
751 & mechanisms, 2015. **8**(1): p. 1-16.

752

753